Fluid theory and simulations of instabilities, turbulent transport and coherent structures in partially-magnetized...

Article *in* Plasma Physics and Controlled Fusion · January 2017

DOI: 10.1088/0741-3335/59/1/014041

10 authors, including:

Andrei Smolyakov
University of Saskatchewan
302 PUBLICATIONS **2,867** CITATIONS
SEE PROFILE

Y. Raitses
Princeton University
290 PUBLICATIONS **2,814** CITATIONS
SEE PROFILE

Igor Kaganovich
Princeton University
321 PUBLICATIONS **2,585** CITATIONS
SEE PROFILE

V. P. Lakhin
Kurchatov Institute
66 PUBLICATIONS **419** CITATIONS
SEE PROFILE

Fluid theory and simulations of instabilities, turbulent transport and coherent structures in partially-magnetized plasmas of $\mathbf{E} \times \mathbf{B}$ discharges

2017 Plasma Phys. Control. Fusion 59 014041

(http://iopscience.iop.org/0741-3335/59/1/014041)

IOP Publishing Plasma Physics and Controlled Fusion
Plasma Phys. Control. Fusion **59** (2017) 014041 (13pp) doi:10.1088/0741-3335/59/1/014041

Fluid theory and simulations of instabilities, turbulent transport and coherent structures in partially-magnetized plasmas of $\mathbf{E}\times\mathbf{B}$ discharges

A I Smolyakov[1,5], O Chapurin[1], W Frias[1], O Koshkarov[1], I Romadanov[1], T Tang[1], M Umansky[2], Y Raitses[3], I D Kaganovich[3] and V P Lakhin[4]

[1] Department of Physics and Engineering Physics, University of Saskatchewan, 116 Science Place, Saskatoon SK S7N 5E2, Canada
[2] Lawrence Livermore National Laboratory, Livermore, CA 94550, USA
[3] Princeton Plasma Physics Laboratory, PO Box 451, Princeton, NJ 08543, USA
[4] NRC 'Kurchatov Institute', 1 Kurchatov Sqr., Moscow 123182, Russian Federation

E-mail: andrei.smolyakov@usask.ca

Received 15 August 2016, revised 4 October 2016
Accepted for publication 10 October 2016
Published 16 November 2016

Abstract

Partially-magnetized plasmas with magnetized electrons and non-magnetized ions are common in Hall thrusters for electric propulsion and magnetron material processing devices. These plasmas are usually in strongly non-equilibrium state due to presence of crossed electric and magnetic fields, inhomogeneities of plasma density, temperature, magnetic field and beams of accelerated ions. Free energy from these sources make such plasmas prone to various instabilities resulting in turbulence, anomalous transport, and appearance of coherent structures as found in experiments. This paper provides an overview of instabilities that exist in such plasmas. A nonlinear fluid model has been developed for description of the Simon-Hoh, lower-hybrid and ion-sound instabilities. The model also incorporates electron gyroviscosity describing the effects of finite electron temperature. The nonlinear fluid model has been implemented in the BOUT++ framework. The results of nonlinear simulations are presented demonstrating turbulence, anomalous current and tendency toward the formation of coherent structures.

Keywords: $\mathbf{E}\times\mathbf{B}$ discharges, instabilties, turbulence, anomalous transport, Hall thrusters, electric propulsion, magnetrons

S Online supplementary data available from stacks.iop.org/PPCF/59/014041/mmedia

(Some figures may appear in colour only in the online journal)

1. Introduction

Plasma systems with electron drift in crossed electric and magnetic fields are of interest for a number of applications such as space propulsion, plasma sources for material processing and magnetic filters for ion extraction and separation. In these devices, the strength of the external magnetic field is such that the electrons are magnetized but ions are not, so that $\rho_e \ll L$ and $\rho_i \gg L$, where L is the characteristic length scale of the plasma region in the device. For the purposes of this article we will refer to such regimes as partially-magnetized or Hall plasmas. In these plasmas, the discharge is supported by the electron current due to $\mathbf{E}\times\mathbf{B}$ drift, while ions, due to large Larmor radius, can be accelerated by externally applied

[5] Also at NRC Kurchatov Institute, 1 Kurchatov Sqr., Moscow 123182, Russian Federation

electric field **E** and extracted from the discharge. These are common operation regimes in Hall plasma thrusters [1, 2], magnetron devices for material processing [3], magnetic filters [4] and Penning type plasma sources [5]. Similar plasma parameters regimes with strong $\mathbf{E}\times\mathbf{B}$ flows are also of interest for space plasma physics [6–8].

Despite long history of successful application of Hall thrusters and other Hall plasma sources, some aspects of their operation are still poorly understood. One notable problem is the anomalous electron mobility, which exceeds the classical collisional values by several orders of magnitude [9–15]. Hall plasmas exhibit numerous oscillations in a wide range of frequencies [16–19], and it is generally believed that turbulent oscillations are responsible for anomalous transport in Hall plasmas. Hall plasma devices also demonstrate the appearance of low frequency coherent structures [20–23] which are likely the result of plasma nonlinear self-organization. Therefore, the problem of anomalous electron mobility in Hall plasmas is another incarnation of a more general problem of plasma turbulence, anomalous transport and heating. In this paper, we review basic mechanisms of instabilities that may be operative in such plasmas and resulting in plasma turbulence. We formulate the nonlinear fluid model describing such turbulence and present results of nonlinear fluid simulations demonstrating turbulent behavior, anomalous transport and coherent structures.

The equilibrium $\mathbf{E}\times\mathbf{B}$ electron drift, plasma density, temperature and magnetic field gradients, and ion flow are all sources of plasma instabilities in Hall plasmas [24]. The gradient-drift instability, related to the anti-drift mode [25], and lower-hybrid instability of Hall plasma with transverse current [26–28] are thought to be particularly important. The long wavelength $\mathbf{E}\times\mathbf{B}$ instability driven by the combination of the magnetic field and density gradients was experimentally and theoretically identified as a possible source of fluctuations and anomalous mobility in Hall plasma thrusters [29–32] and later in Penning discharges [33]. In general, this instability can be considered as a collisionless version of the collisional Simon-Hoh instability [34, 35]. The long wavelength gradient-drift instabilities are usually considered in neglect of the electron inertia. However, for higher frequencies and shorter wavelengths the effects of the electron inertia become important which leads to coupling to the lower-hydrid modes. The effects of plasma and magnetic field gradients on the lower-hybrid instability were earlier studied in kinetic theory in [36–39]. Here we present an advanced nonlinear fluid model that incorporates electron gyroviscosity and self-consistently describes both long-wavelength gradient-drift and lower-hybrid instabilities. In fact, we show that gradient-drift instability smoothly transits into the lower-hybrid mode at shorter wavelengths $k_\perp\rho_e\simeq 1$.

The short wavelength lower-hybrid modes are also a special case of more general beam cyclotron instabilities [40–42], in which higher cyclotron harmonics are included. The nonlinear stage of such cyclotron instabilities, driven by the transverse current was analyzed in [40, 41, 43], where it was concluded that these small scale modes saturate at relatively low amplitude due to ion trapping. It was also shown that a number of effects such as collisions, finite value of the wavevector along the magnetic field, nonlinear diffusion also result in smoothing out the cyclotron resonances and the mode transits into a slow ion-sound instability. This mode has been recently considered as a possible source of short-wavelength fluctuations and anomalous mobility in Hall thrusters [19, 42, 44–47]. For a recent review of physics of the electron–cyclotron instability, numerical simulations results and related experiments see [48] and references therein.

Our fluid model in the short-wave-length limit, $k_\perp^2\rho_e^2\gg 1$, correctly describes the transition to the ion sound mode. In plasmas with unmagnetized ions, pure ion sound mode exists for finite values of the wave-vector along the magnetic field, $k_\parallel v_{Te}>\omega$. In the lowest order, coupling of the ion sound mode to the equilibrium $\mathbf{E}\times\mathbf{B}$ flow of electrons is weak. This coupling, however, can be enhanced by electron-neutral collisions resulting in the collisional instability of the ion sound waves in plasma with the equilibrium $\mathbf{E}\times\mathbf{B}$ flow [49]. The instability of a similar nature occurs in the collisionless regime due to the inverse Landau damping associated with the $\mathbf{E}\times\mathbf{B}$ electron current. In a finite length plasma, the electron current into the sheath leads to a specific resistive effect: sheath resistivity [50], which may result in the wall induced (resistive) instabilities [49, 51]. General case of the sheath near the dielectric wall was considered in [49].

The full picture of instabilities in Hall plasmas is complex and, for typical experimental conditions, likely involves a number of interacting modes which require numerical simulations. Particle-in-cell kinetic simulations that offer a first principles description and have provided valuable results on $\mathbf{E}\times\mathbf{B}$ plasma discharges [52–55] could be the most realistic approach to study the experimental conditions. However PIC simulations also could be difficult to interpret, especially when practical limitations of the modern computer capabilities and available resources are taken into account. On the other hand, fluid simulations are faster numerical tools that can provide deep insights into the nonlinear plasma dynamics. They are easier to interpret and provide much greater flexibility in separating various physics elements. We have developed a set of nonlinear fluid codes to investigate the turbulent fluctuations and transport in Hall plasmas relevant to electric propulsion [56, 57]. These fluid simulations capabilities are being developed in conjunction with kinetic particle-in-cell simulations [58]. Here we describe the results of our fluid simulations of turbulence and anomalous transport relevant to electric propulsion, magnetron plasma sources, and magnetic filters.

In this paper we mostly consider 2D plasma dynamics in the plane perpendicular to the magnetic field and do not consider any 3D effects, assuming that $k_\parallel=0$, $k_\parallel$ is the wavevector along the equilibrium magnetic field. Therefore, we do not consider here the modified two-stream instability [41, 59] and related modes, which require a finite component of the wavevector along the magnetic field. Our emphasis in this paper is on higher frequency modes. Thus we do not consider here the low-frequency oscillations and instabilities that involve ionization processes such as breathing modes [60]. For the description of some instabilities due to the ionization see [61,

62] and references therein. A useful summary of experimental studies of low-frequency oscillations is provided in [63].

The overview of instabilities in this paper is oriented toward the understanding the behavior of plasmas in such systems as Hall thrusters [64–66], magnetrons [67] and magnetic filters [4]. In most typical configurations these devices involve electron $\mathbf{E}\times\mathbf{B}$ current, beams of accelerated ions and plasma parameters gradients as sources of plasma instabilities. One particular case, namely Penning discharge geometry, does not involve the accelerated ions nor the magnetic field gradient. The experiments with Penning discharges [8, 23, 68] have been performed to study the effects of plasma density gradients, shear of the $\mathbf{E}\times\mathbf{B}$ flows and neutral pressure. In this paper, unless noted otherwise, various instabilities as presented in figures 1–4 are characterized for plasma parameters of the Penning discharge in [23]. Unstable eigen-modes for the parameters of the Hall thruster from [65] are characterised in [69]. We have developed a simple solver that can be used to evaluate real frequency and growth rate for the local instabilities discussed in this paper. The solver is described in [70] and also available online as a the citation to supplementary material to this paper. Local models are useful in providing physics insight and developing intuition on presence of instabilities. It is important to note though, that in plasmas with strongly inhomogeneous parameters, the properties of nonlocal modes can significantly differ from the predictions of the local models [69]. In general, nonlocal and nonlinear analysis is required to predict the occurance of fluctuations, its characteristics and consequences such as anomalous transport. In this paper, we describe the physics of the instabilities relevant to partially magnetized plasmas in $\mathbf{E}\times\mathbf{B}$ discharges and present nonlinear simulations of turbulence resulting from such instabilities.

The rest of the paper is organised as follows. In section 2, the analytical models and results of the linear eigen-value analysis are presented. Section 3 is devoted to the description of nonlinear model and results of nonlinear simulations.

2. Basic plasma dynamics models and instabilities

In this section, the set of basic fluid equations for plasma dynamics in partially magnetised Hall plasmas is formulated. We use a generic geometry configuration in which the equilibrium magnetic field is directed along the z axis, $\mathbf{B}_0 = B_0\hat{\mathbf{z}}$, the equilibrium electric field and density (and possibly magnetic field) gradients are in the x direction, $\mathbf{E}_0 = E_0\hat{\mathbf{x}}$, $n_0 = n_0(x)$. The azimuthal (periodic) direction is taken along the y axis. In application to the cylindrical Hall thrusters, the magnetic field would be directed radially (z-axis), the electric field along the axis of the thruster (x-axis), and the y-direction is azimuthal. For the cylindrical magnetron configuration (Penning discharge geometry), the magnetic field is axial (z-direction), and electric field and density gradients are radial (x-direction) and y-direction is azimuthal. Plasma is assumed to be quasineutral and the perturbed electric field is electrostatic. Plasma is quasineutral at the length scales below the Debye length, $k^2\lambda_{De}^2 < 1$. For typical parameters in [23], $B_0 = 5\times10^{-3}$ T, $T_e = 10$ eV, and $n_e = 10^{18}$ m^{-3}, we have $\lambda_{De} = 2.35\times10^{-5}$ m $\rho_e = 6.73\times10^{-4}$ m, and $\rho_e^2/\lambda_{De}^2 \simeq 10^3$. Thus, for $\rho_e^2/\lambda_{De}^2 > 1$, quasineutral approximation remains valid for $k_\perp^2\rho_e^2 \geqslant 1$. The electrostatic approximation is valid for small scale fluctuations with $k^2c^2/\omega_{pe}^2 \gg 1$. In the range of $n_e = 10^{17} \div 10^{18}$ m^{-3}, $c/\omega_{pe} \simeq (1.7 \div 0.5)\times10^{-2}$ m, thus, the electromagnetic corrections, related to the magnetosonic waves, will be important only for large scale perturbations with $L \simeq 10^{-2}$ m and larger.

In this section we use the parameters of the Penning discharge experiment [23], to characterise the main instabilities in partially-magnetized plasmas.

2.1. Ion dynamics

In partially–magnetized plasmas, the ion Larmor radius is typically larger than the system size and the ion cyclotron frequency is lower than the oscillation frequencies. These conditions allow to neglect the effects of the magnetic field on ions in the simplest model. For some phenomena, the magnetic field effect on ions is still important. In these regimes, ion dynamics is strongly nonlocal and generally require kinetic theory which is outside the scope of this paper.

Basic equations for cold unmagnetized ions are the continuity and momentum equations:

$$\frac{\partial n_i}{\partial t} + \nabla\cdot(n_i\mathbf{v}_i) = 0, \tag{1}$$

$$\frac{\partial \mathbf{v}_i}{\partial t} + (\mathbf{v}_i\cdot\nabla)\mathbf{v}_i = -\frac{e}{m_i}\nabla\phi. \tag{2}$$

For linear perturbations with $(\tilde{n},\phi)\sim\exp(-i\omega t + i\mathbf{k}\cdot\mathbf{x})$, the system of equations (1)–(2) gives the following expression for the perturbed ion density

$$\frac{\tilde{n}}{n_0} = \frac{k^2\tilde{v}_i^2}{(\omega - \mathbf{k}\cdot\mathbf{v}_{0i})^2}, \tag{3}$$

where $\tilde{v}_i = (e\tilde{\phi}/m_i)^{1/2}$ is the oscillatory ion velocity in the perturbed field and $\mathbf{v}_{0i}$ is the equilibrium ion velocity.

2.2. Destabilization of the anti-drift mode by the electron and ion flows

Hall plasmas with unmagnetized ions do not support the standard drift waves. However, the density gradient and ion inertia result in the so-called anti-drift mode [25]. Formally, this mode occurs only for the perturbations which are constant along the magnetic field, $\mathbf{b}\cdot\nabla = \mathbf{0}$, where $\mathbf{b} = \mathbf{B}/B$ is the unit vector along the magnetic field. In fact, in finite length systems, where the magnetic field lines are terminated by boundaries, the perturbations also become two-dimensional (in the plane perpendicular to the magnetic field) when the electron pressure quickly equilibrates along the magnetic field due to fast electron thermal motion, for $\omega \ll k_\parallel v_{Te}$, where $v_{Te} = \sqrt{2T_e/m_e}$ is the electron thermal velocity and $k_\parallel$ is the component of the wave vector along the magnetic field. In this state, the difference between the electron density and the potential is constant along the magnetic field but remains a function of the transverse (perpendicular to the magnetic field) coordinates. Then,

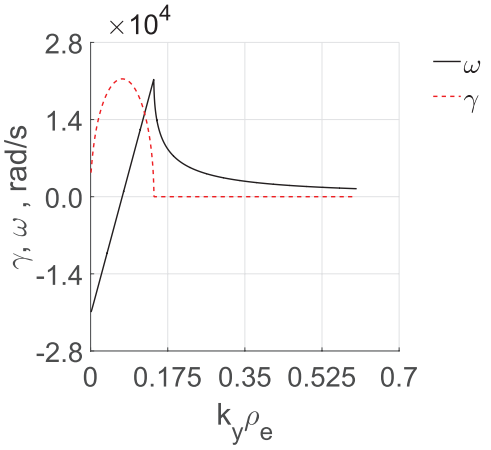

Figure 1. Frequency and growth rate of the anti-drift mode in equation (9) destabilized by the ion drift as a function of $k_y\rho_e$ for $v_{i0} < 0$, $v_{i0} = -2 \times 10^4$ m s^{-1}, $\omega_0 = 0$, $L_n < 0$, $k_x\rho_e = -7.5 \cdot 10^{-4}$, $\rho_e = \sqrt{T_e/m_e\omega_{ce}^2}$.

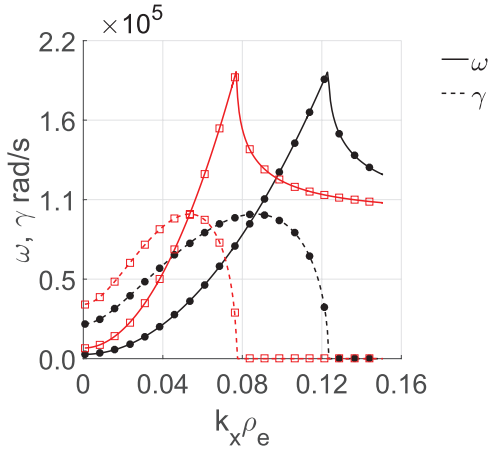

Figure 2. Frequency and growth rate of the anti-drift mode destabilized by the electron flow, $v_{i0} = 0$ as a function of the transverse wave-vector $k_x\rho_e$ for $L_n = -0.04$ m (squares) and $L_n = -0.1$ m (dots).

the slow electron motion in the perpendicular plane such as that due to the $\mathbf{E} \times \mathbf{B}$ and diamagnetic drifts determine the density and potential evolution, which effectively means $k_\parallel = 0$.

In the simplest case and neglecting electron inertia, the electron response is due to the electron $\mathbf{E} \times \mathbf{B}$ drift

$$\frac{\partial \tilde{n}}{\partial t} + \mathbf{v}_E^0 \cdot \nabla \tilde{n} + \tilde{\mathbf{v}}_E \cdot \nabla n_0 = 0, \tag{4}$$

giving

$$\frac{\tilde{n}}{n_0} = \frac{\omega_*}{\omega - \omega_0}\frac{e\tilde{\phi}}{T_e} = -\frac{1}{(\omega - \omega_0)\omega_{ci}}\frac{k_y\tilde{v}_i^2}{L_n}, \tag{5}$$

where $\omega_0 = k_y v_{E0}$, $\omega_* = k_y v_*$, $v_{E0} = -E_0/B_0$, $v_* = -cT_e/(eB_0L_n)$, $L_n^{-1} = n_0'/n_0$. Using the perturbed ion density from equation (3), and neglecting the ion flow, one gets for quasineutral oscillations

$$\frac{k^2c_s^2}{\omega^2} = \frac{\omega_*}{\omega - \omega_0}. \tag{6}$$

The stable anti-drift mode follows for $\omega_0 = 0 : \omega = k^2c_s^2/\omega_*$ [25]. In fact, the anti-drift mode does not depend on the electron temperature and the eigen-mode frequency can be written as: $\omega = -k^2L_n\omega_{ci}/k_y$. Note that for $\omega_* \to 0$, the electron inertia and parallel dynamics which were neglected in the equation (4), will have to be included.

The collisionless Simon-Hoh instability [33, 71–73] occurs due to the destabilization of the anti-drift mode by the electron flow. The electron response is modified by the $\mathbf{E} \times \mathbf{B}$ Doppler shift: $\omega \to \omega - \omega_0$. From (6), one can easily see the instability criteria for $\omega < \omega_0$ in the form: $\omega_*/\omega_0 > 0$. The latter instability condition can be written in general form as

$$\left(\mathbf{k} \cdot \mathbf{b} \times \frac{\nabla n_0}{n_0}\right)(\mathbf{k} \cdot \mathbf{b} \times \mathbf{E}_0) > 0. \tag{7}$$

For a simple case when $\mathbf{b} = \hat{\mathbf{z}}$, $\mathbf{k} = k_y\hat{\mathbf{y}}$ and $n_0 = n_0(x)$ this is written as $\mathbf{E}_0 \cdot \nabla n_0 > 0$.

The equilibrium ion velocity introduces the Doppler shift in the ion response, $\omega \to \omega - \mathbf{k} \cdot \mathbf{v}_{0i}$. This regime, called the modified Simon-Hoh instability, has been studied in [73–75] with emphasis on the effects of large orbits of trapped ions in Penning discharge geometry. Note however, that for the Hall truster and plane magnetron situations, the ions are not trapped and may have finite velocity due to acceleration in the equilibrium electric field. The contribution of a finite ion velocity $\mathbf{v}_{0i}$, modifies the real part of the frequency and, for larger values of $\mathbf{v}_{0i}$, a new instability may set in. This can be seen from general dispersion relation

$$\frac{\omega_*}{\omega - \omega_0} = \frac{k^2c_s^2}{(\omega - \omega_{0i})^2}, \tag{8}$$

which gives

$$\omega = \omega_{0i} + \frac{k^2c_s^2}{2\omega_*} + \sqrt{\frac{k^4c_s^4}{4\omega_*^2} + \frac{k^2c_s^2}{\omega_*}(\omega_{0i} - \omega_0)}\,. \tag{9}$$

There exist two separate mechanisms of destabilization, associated with the equilibrium drift of electrons ω_0, and ions ω_{0i}, respectively. Finite electron flow is destabilizing for $\omega_0/\omega_* > 0$. This condition is independent of the sign of the azimuthal wave vector k_y and can be written as $\mathbf{E}_0 \cdot \nabla n_0 > 0$. More precisely, the condition $v_{E0} > (k^2/4k_y^2)\omega_{ci}L_n$ is required for the instability. For the modes with the lowest instability threshold, $k_x = 0$, see figure 2, this condition becomes $|v_{E0}| > \omega_{ci}|L_n|/4$, which easily satisfied in most $\mathbf{E} \times \mathbf{B}$ discharge plasmas. Note that for $B_0 = 5 \times 10^{-3}$ T, xenon plasma and $|L_n| = 0.04$ m, $\omega_{ci}|L_n|/4 \simeq 37$ m s^{-1}.

The equilibrium ion flow is destabilizing for $\omega_{0i}/\omega_* < 0$, or equivalently for $k_x v_{0i}L_n/k_y > 0$. This means that for the conditions of the Hall thruster with $\mathbf{v}_{0i} = v_{0i}\hat{\mathbf{x}}$, $v_{0i} > 0$, the unstable modes should have definite helicity: $k_xL_n/k_y > 0$. A more accurate instability criterion has the form

$$\frac{\omega_{0i}}{\omega_*} < -\frac{k^2c_s^2}{4\omega_*^2}, \tag{10}$$

which can also be written as

$$v_{0\mathrm{i}} > \frac{1}{4}\left(\frac{k_x}{k_y}+\frac{k_y}{k_x}\right)\omega_{\mathrm{ci}}L_n, \tag{11}$$

assuming the condition $k_xL_n/k_y > 0$.

The growth rate and real part of the anti-drift mode destabilized by the electron flow has a linear scaling with the wave-vector, $(\omega_r, \gamma) \sim k_y$ [76]. The ion flow driven instability has more complex dependence on k_y, see figure 1.

It is interesting to note that for $k_xv_{0\mathrm{i}}L_n/k_y > 0$, the instability may occur in two different situations; simultaneous change of the sign of k_y and k_x does not change the growth rate, but affects the sign of the real part of the frequency. The eigen-frequency of of the ion driven instability is shown in figure 1 for negative v_{i0}, $k_x < 0$ and $L_n < 0$, k_y is taken to be positive.

The Simon-Hoh instability is usually thought of as a relatively low frequency mode, $\omega < \omega_0$ [77]. It is important to note however that for a given value of the azimuthal wave-vector k_y, the eigen-value of the destabilized anti-drift mode is a non-monotonous function of the axial wave vector k_x [69]. The modes with $k_x = 0$ have the lowest instability threshold. At fixed k_y (and $\omega_{0\mathrm{i}} = 0$), the growth rate is increasing with k_x and reaches the maximum at

$$\frac{k^2c_s^2}{2\omega_*} = \omega_0. \tag{12}$$

At this point, the real part of the frequency and growth rate are equal to ω_0, $\omega = \omega_0 + \mathrm{i}\omega_0$. For higher values of k_x the growth rate decreases and finally the mode is stabilized. For the case of pure electron flow destabilization, the eigen-frequency is shown in figure 2 as a function of k_x for two values of the L_n parameter. Thus, for the eigen-modes with a maximum growth rate [69], the frequency follows k_yv_{E0} scaling similarly to the experimental data in [11]. For the ion flow destabilization ($\omega_0 = 0$), the maximum growth rate depends on the ratio of ω_* and k_yc_s.

2.3. Electron dynamics including inertia and gyroviscosity

As was shown in [69], the growth rate and real part of the unstable anti-drift modes reaches the $\omega_0 = k_yv_{E0}$ value, which means that even for low azimuthal wave vector k_y, the mode frequency may become comparable to the lower-hybrid frequency. In this case, electron inertia has to be included which couples Simon-Hoh instability to the lower-hybrid waves. At shorter wavelengths, the finite electron temperature (electron Larmor radius) effects also become important. In general, the regimes with large values of the wave vector $k_\perp^2\rho_\mathrm{e}^2 \gg 1$ have to be described by kinetic theory. It is however, possible to describe the finite electron Larmor radius (FLR) effects via the electron gyroviscosity. In the limit of finite but small $k_\perp^2\rho_\mathrm{e}^2 < 1$ the gyroviscosity provides asymptotically correct description of the electron FLR. In the limit of large, $k_\perp^2\rho_\mathrm{e}^2 \geqslant 1$, the gyroviscosity provides qualitatively correct behaviour which is equivalent to the Padé type approximants (for $k_\perp^2\rho_\mathrm{e}^2 \gg 1$) for the Bessel functions appearing in the exact kinetic theory [78].

The most general electron momentum balance equation, including the electron inertia and gyroviscosity is written in the form

$$m_\mathrm{e}n_\mathrm{e}\frac{\mathrm{d}\mathbf{v}_\mathrm{e}}{\mathrm{d}t} = en_\mathrm{e}(-\nabla\phi + \frac{1}{c}\mathbf{v}_\mathrm{e}\times\mathbf{B}) - \nabla p_\mathrm{e} - \nabla\cdot\mathbf{\Pi} - m_\mathrm{e}n_\mathrm{e}\nu\mathbf{v}_\mathrm{e}, \tag{13}$$

where the fluid (substantive) derivative is

$$\frac{\mathrm{d}}{\mathrm{d}t} = \frac{\partial}{\partial t} + \mathbf{v}_\mathrm{e}\cdot\nabla, \tag{14}$$

and $\mathbf{\Pi}$ is the viscosity tensor. We consider the electron collisions with stationary neutral atoms resulting in the friction force described by the last term in equation (13).

The electron dynamics is considerably simplified by employing the low frequency ordering $\omega \ll \omega_{\mathrm{ce}}$. In this ordering, for the electron viscosity suffices to consider only collisionless gyroviscosity tensor $\mathbf{\Pi}_\mathrm{g}$. Assuming that $\mathrm{d}/\mathrm{d}t \ll \omega_{\mathrm{ce}}$, the electron velocity from equation (13) can be written as

$$\mathbf{v}_{\mathrm{e}\perp} = \mathbf{v}_E + \mathbf{v}_{\mathrm{pe}} + \mathbf{v}_I + \mathbf{v}_\nu + \mathbf{v}_{\Pi_\mathrm{g}}, \tag{15}$$

where $\mathbf{v}_E$ is the $\mathbf{E}\times\mathbf{B}$ drift velocity, $\mathbf{v}_{\mathrm{pe}}$ is the diamagnetic drift velocity and $\mathbf{v}_I$, $\mathbf{v}_\nu$ and $\mathbf{v}_{\Pi_\mathrm{g}}$ are the drift velocities associated with the inertia, collisions and gyroviscosity tensor,

$$\mathbf{v}_E = \frac{c\mathbf{b}}{B_0}\times\nabla_\perp\phi, \mathbf{v}_{\mathrm{pe}} = -\frac{1}{en}\frac{\mathbf{b}}{B_0}\times\nabla_\perp p_\mathrm{e}, \tag{16}$$

$$\mathbf{v}_I = -\frac{1}{\omega_{\mathrm{ce}}}\mathbf{b}\times\frac{\mathrm{d}}{\mathrm{d}t}(\mathbf{v}_\mathbf{E}+\mathbf{v}_{\mathrm{pe}}), \tag{17}$$

$$\mathbf{v}_\nu = \frac{\nu}{\omega_{\mathrm{ce}}}\mathbf{b}\times\left(\mathbf{v}_\mathbf{E}+\mathbf{v}_{\mathrm{pe}}\right), \mathbf{v}_{\Pi_\mathrm{g}} = -\frac{c}{enB_0}\mathbf{b}\times\nabla\cdot\mathbf{\Pi}_\mathrm{g}. \tag{18}$$

The gyroviscosity tensor in the last equation is given by [79–81]

$$\mathbf{\Pi}_\mathrm{g} = \frac{1}{\omega_{\mathrm{ce}}}\hat{\mathbf{K}}^{-1}\left(\left[p\nabla\mathbf{v} + p(\nabla\mathbf{v})^T\right] + \frac{2}{5}\left[\nabla\mathbf{q} + (\nabla\mathbf{q})^T\right]\right), \tag{19}$$

where the operator $\hat{\mathbf{K}}^{-1}$ acting on a (symmetric) tensor $\mathbf{A}$ is

$$\hat{\mathbf{K}}^{-1}\mathbf{A} = \frac{1}{4}\{\left[\mathbf{b}\times\mathbf{A}\cdot(\mathbf{1}+3\mathbf{bb})\right] + \left[\mathbf{b}\times\mathbf{A}\cdot(\mathbf{1}+3\mathbf{bb})\right]^T\}. \tag{20}$$

In the expression for $\mathbf{\Pi}_\mathrm{g}$, $\mathbf{v} = \mathbf{v}_E + \mathbf{v}_{\mathrm{pe}}$ and the heat flux $\mathbf{q} = -5/2p_\mathrm{e}\mathbf{b}\times\nabla T_\mathrm{e}/(eB_0)$.

The gyroviscous force provides the same order contribution to the momentum balance equation as the inertia term. There are certain cancellations between two terms, the so called gyroviscous cancellation. The general form of the gyroviscous cancellation can be written as [80]

$$m_\mathrm{e}n_\mathrm{e}(\mathbf{v}_{\mathrm{pe}}\cdot\nabla)\mathbf{v}_{\mathrm{e}\perp} + \nabla\cdot\mathbf{\Pi}_\mathrm{g} = \nabla\xi', \tag{21}$$

where ξ' is some scalar function.

Taking into account the gyroviscous cancellation from equation (21), for isothermal electrons, the electron velocity is

$$\mathbf{v}_{\mathrm{e}\perp} = \mathbf{v}^{(0)} + \mathbf{v}^{(1)}, \tag{22}$$

$$\mathbf{v}^{(0)} = \frac{c\mathbf{b}}{B_0} \times \nabla_\perp \phi - \frac{cT_e}{en_e}\frac{\mathbf{b}}{B_0} \times \nabla_\perp n = \mathbf{v}_E + \mathbf{v}_{pe}, \quad (23)$$

$$\mathbf{v}^{(1)} = -\frac{1}{\omega_{ce}}\left(\frac{\partial}{\partial t} + \mathbf{v}_E \cdot \nabla + \nu\right)(\mathbf{v}_E + \mathbf{v}_{pe}), \quad (24)$$

and the electron continuity equation

$$\frac{\partial \tilde{n}}{\partial t} + \mathbf{v}_E \cdot \nabla n + \nabla \cdot (n\mathbf{v}^{(1)}) = 0.$$

Then, with (22)–(24), general equation for the perturbed electron density can be written in the form

$$\frac{\partial}{\partial t}\left(\tilde{n} - \rho_e^2 \nabla_\perp^2 \tilde{n}\right) - \nu\rho_e^2\nabla_\perp^2\tilde{n} + \mathbf{v}_E^0 \cdot \nabla\tilde{n} + \tilde{\mathbf{v}}_E \cdot \nabla n_0 + \tilde{\mathbf{v}}_E \cdot \nabla\tilde{n} + n_0\rho_e^2\nabla_\perp^2\frac{\partial}{\partial t}\left(\frac{e\widetilde{\phi}}{T_e}\right) + \nu n_0\rho_e^2\nabla_\perp^2\frac{e\widetilde{\phi}}{T_e} + \frac{n_0 c}{B_0\omega_{ce}}(\mathbf{v}_E \cdot \nabla)\nabla_\perp^2\phi - \frac{T_e c}{eB_0\omega_{ce}}\nabla \cdot [(\mathbf{v}_E \cdot \nabla)\nabla_\perp n] = 0. \quad (25)$$

In the last two terms in this equation, variables $\mathbf{v}_E$, ϕ and n contain both equilibrium and perturbed parts. One has

$$(\mathbf{v}_E \cdot \nabla)\nabla_\perp^2\phi = (\mathbf{v}_E^0 \cdot \nabla)\nabla_\perp^2\widetilde{\phi} + (\tilde{\mathbf{v}}_E \cdot \nabla)\nabla_\perp^2\widetilde{\phi} + (\tilde{\mathbf{v}}_E \cdot \nabla)\phi_0'', \quad (26)$$

where $\phi_0'' = \mathrm{d}^2\phi_0/\mathrm{d}x^2$. Similarly,

$$\nabla \cdot [(\mathbf{v}_E \cdot \nabla)\nabla_\perp n] = \nabla \cdot [(\mathbf{v}_E^0 \cdot \nabla)\nabla_\perp\tilde{n}] + \nabla \cdot [(\tilde{\mathbf{v}}_E \cdot \nabla)\nabla_\perp\tilde{n}] + \nabla \cdot [(\tilde{\mathbf{v}}_E \cdot \nabla)\nabla_\perp n_0]. \quad (27)$$

The nonlinear terms can conveniently be written in the form using the Poisson brackets: $\{a, b\} = (\partial a/\partial x)(\partial b/\partial y) - (\partial b/\partial x)(\partial a/\partial y)$. Therefore,

$$(\tilde{\mathbf{v}}_E \cdot \nabla)\nabla_\perp^2\widetilde{\phi} = \frac{c}{B_0}\{\widetilde{\phi}, \nabla_\perp^2\widetilde{\phi}\}, \quad (28)$$

and

$$\nabla \cdot [(\tilde{\mathbf{v}}_E \cdot \nabla)\nabla_\perp\tilde{n}] = \frac{c}{B_0}\nabla \cdot \{\widetilde{\phi}, \nabla_\perp\tilde{n}\}. \quad (29)$$

The last terms in equations (26) and (27) are related to the shear of the equilibrium flow $\mathbf{v}_E^0$ and the higher order derivatives of the equilibrium density. The shear of the equilibrium flow (the last term in equation (26)) may result in the Kelvin–Helmholtz type instabilities. Such instabilities in application to Hall thruster were studied in [82, 83] (related modes were also considered in [83]). Note that the gyroviscosity adds new terms related to the higher derivatives of the equlibrium density. Similarly to the shear flow effects, the gradients of the equilibrium density will affect the stability of Hall plasma systems and, in general, require nonlocal analysis, which is outside of the scope of this paper.

In linear approximation and using the Boussinesque approximation (neglecting the terms related to the shear of the equilibrium flow $\mathbf{v}_E^0$ and higher derivatives of the equilibrium density), one obtains from (25)) the following expression for the perturbed electron density

$$\frac{\tilde{n}}{n_0} = \frac{\omega_* + k_\perp^2\rho_e^2(\omega - \omega_0 + i\nu_{en})}{\omega - \omega_0 + k_\perp^2\rho_e^2(\omega - \omega_0 + i\nu_{en})}\frac{e\phi}{T_e}. \quad (30)$$

where $\omega_0 = \mathbf{k} \cdot \mathbf{v}_E^0$ is the Doppler shift frequency due to the equilibrium electron flow, and $\rho_e^2 = cT_e/(eB_0\omega_{ce})$ is the electron Larmor radius.

2.4. Lower-hybrid instability and transition to the ion sound mode for $k_\perp^2\rho_e^2 \gg 1$

The lower-hybrid mode appears as a result of the balance between inertia of unmagnetized ions and transverse inertia of magnetized electrons across the magnetic field. In neglect of the drift terms, electron gyroviscosity and collisions, the transverse electron inertia results in the perturbed electron density in the form: $\tilde{n}/n_0 = k_\perp^2\rho_e^2(e\phi/T_e)$. Quasineutrality and ion density from (3) give the basic lower-hybrid mode: $(\omega - k_x v_{0i})^2 = \omega_{LH}^2 \equiv \omega_{ce}\omega_{ci}$. General expression for the perturbed electron density in equation (30) results in the following general dispersion equation for quasineutral oscillations

$$\frac{\omega_* + k_\perp^2\rho_e^2(\omega - \omega_0 + i\nu_{en})}{\omega - \omega_0 + k_\perp^2\rho_e^2(\omega - \omega_0 + i\nu_{en})} = \frac{k_\perp^2 c_s^2}{(\omega - k_x v_0)^2}. \quad (31)$$

This dispersion equation describes modifications of the basic lower-hybrid mode due to density gradient, equilibrium $\mathbf{E} \times \mathbf{B}$ drift, collisions and effects of finite electron Larmor radius (via the gyroviscosity tensor). The density gradient, equilibrium $\mathbf{E} \times \mathbf{B}$ electron flow and collisions are the mechanisms of the destabilization of the lower-hybrid mode.

Alternatively, one can consider equation (31) as a high frequency extension of the Simon-Hoh instability. The density gradient is a critical ingredient of the Simon-Hoh instability (as described by equation (6)) in neglect of electron inertia. At the higher frequencies, the mode becomes the lower-hybrid mode destabilized by a density gradient. The transition of the inertia–less Simon-Hoh instability into the lower-hybrid instability is described by the equation

$$\frac{\omega_* + k_\perp^2\rho_e^2(\omega - \omega_0)}{\omega - \omega_0} = \frac{k_\perp^2 c_s^2}{\omega^2}, \quad (32)$$

where the electron gyroviscosity is omitted. The growth rate and real frequency described by this equation are shown in figure 3(a). The transition between Simon-Hoh and lower-hybrid instabilities roughly occurs at $\omega_* \simeq k_\perp^2\rho_e^2\omega_0$.

The lower-hybrid mode in plasmas with $\mathbf{E} \times \mathbf{B}$ can also be destabilized by collisions alone and in absense of the density gradient. Such modes were considered in [84]. Relevant dispersion relation has the form

$$\frac{k_\perp^2\rho_e^2(\omega - \omega_0 + i\nu_{en})}{\omega - \omega_0} = \frac{k_\perp^2 c_s^2}{\omega^2}. \quad (33)$$

Assuming $\omega < \omega_0$ and $\nu < \omega_0$ one has [84]

$$\omega = \pm\,\omega_{LH}\left(1 + \frac{i\nu_{en}}{2\omega_0}\right).$$

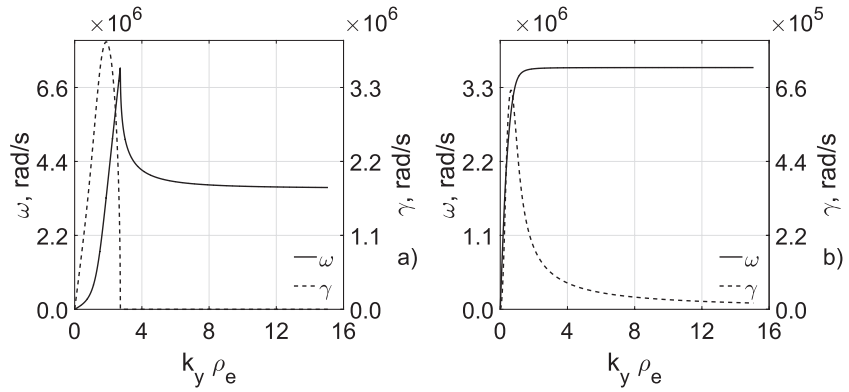

Figure 3. Frequency and growth rate of the lower-hybrid mode as a function of $k_y\rho_e$ at $k_x\rho_e = 7.5 \cdot 10^{-4}$: (a) destabilized by density gradient, $v_* = 1.3 \cdot 10^4$ m s^{-1}, $\nu_e = 0$; (b) destabilized by collisions only, $\omega_* = 0$, $\nu_e = 10^6$ s^{-1}.

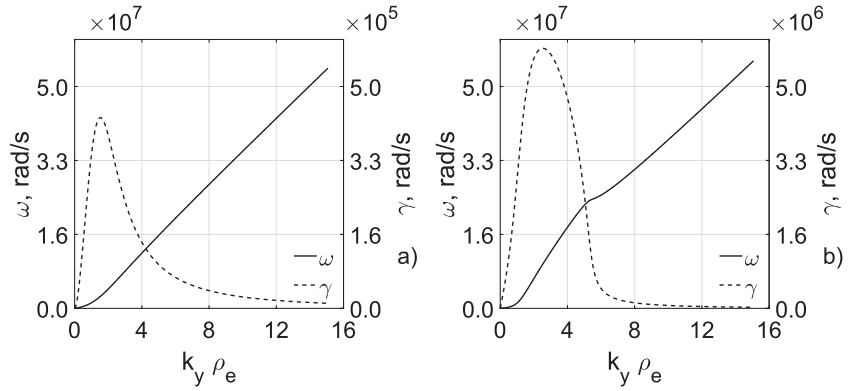

Figure 4. Effect of the gyroviscosity and conversion into the ion sound mode; note that $\omega_r \sim k_y$. (a) Destabilization of the ion-sound mode by density gradient and collisions, $v_* = 1.3 \cdot 10^4$ m s^{-1}, $\nu_e = 10^6$ s^{-1}, $\omega_0 = 0$ (b) Destabilization by density gradient, $\mathbf{E} \times \mathbf{B}$ drift and collisions, $v_* = 1.3 \cdot 10^4$ m s^{-1}, $v_{E0} = 5 \cdot 10^5$ m s^{-1}, $\nu_e = 10^6$ s^{-1}.

The behavior of the growth rate and real part of the frequency from equation (33) is shown in figure 3(b). The maximum growth rate occurs roughly at the point where $\omega_0 \simeq \omega_{\mathrm{LH}}$.

The gyroviscosity has profound effect on the mode behavior at large $k_\perp^2\rho_e^2$. It is easily seen from equation (30) that at large $k_\perp^2\rho_e^2$, the electron response becomes Boltzmann, and the general dispersion equation (31) results in the ion-sound mode, $\omega^2 = k^2c_s^2$. The short wavelength sound mode can be destabilized by drift effects and collisions even in absence of the $\mathbf{E} \times \mathbf{B}$ drift as is shown in figure 4(a). The $\mathbf{E} \times \mathbf{B}$ drift enhances the instability as is shown in figure 4(b). This instability is similar to the appearance of the short wavelength ion sound mode in the kinetic theory of the electron drift cyclotron instability [85–87]. In finite length systems, the ion sound modes can also be destabilized by ion flow effects [88].

2.5. Gradient of the magnetic field effects

The authors have recently revisited the problem of the long wavelength $\mathbf{E} \times \mathbf{B}$ instability in plasmas with inhomogeneous magnetic field and plasma density gradients which was originally studied in [30] and later in [89]. It was shown that quantitative corrections (to the previous theory) are required for the accurate determination of the conditions for the instability and its characteristic frequency [76, 90]. These corrections occur due to full compressibility of the $\mathbf{E} \times \mathbf{B}$ drift in inhomogeneous magnetic field, $\nabla \cdot \mathbf{v}_E \simeq -2\mathbf{v}_E \cdot \nabla \ln B$. It was also shown that the compressibility of the diamagnetic velocity, $\nabla \cdot (n\mathbf{v}_{\mathrm{pe}}) \simeq -2n\mathbf{v}_{\mathrm{pe}} \cdot \nabla \ln B$, results in finite perturbations of the electron temperature. A three-field fluid model that includes density, potential and electron temperature perturbations was developed in [76, 90]. The general dispersion equation that includes the electron inertia, gyroviscosity and effects of the magnetic filed gradients has the form

$$\frac{\omega_* - \omega_D + k_\perp^2\rho_e^2(\omega - \omega_0 + \mathrm{i}\nu_{\mathrm{en}})}{\omega - \omega_D - \omega_0 + k_\perp^2\rho_e^2(\omega - \omega_0 + \mathrm{i}\nu_{\mathrm{en}})} = \frac{k_\perp^2 c_s^2}{(\omega - k_x v_0)^2}. \tag{34}$$

Neglecting electron inertia, the instabilities of some realistic profiles in Hall thrusters were considered in [76].

3. Nonlinear model and simulations

3.1. Ion dynamics

For simulations, nonlinear equations are simplified by separating the equilibrium and perturbed parts: $X = X_0(x) + \widetilde{X}(x, y, t)$. The nonlinear evolution equations are solved for the perturbed quantities $\widetilde{X}(x, y, t)$. The equilibrium part $X_0(x)$ is assumed to be fixed. Here, we consider the case of the uniform

electric field $\mathbf{E}_0 = -\nabla\phi_0$, and a uniform gradient of plasma density.

The density evolution equation for ions has the form

$$\left(\frac{\partial}{\partial t} + \mathbf{v}_0\cdot\nabla\right)\tilde{n} + \tilde{\mathbf{v}}\cdot\nabla n_0 + \tilde{n}\nabla\cdot\mathbf{v}_0 + n_0\nabla\cdot\tilde{\mathbf{v}} + \nabla\cdot(\tilde{n}\tilde{\mathbf{v}}) = 0. \tag{35}$$

The equation of motion for cold ions is

$$\left(\frac{\partial\tilde{\mathbf{v}}}{\partial t} + \mathbf{v}_0\cdot\nabla\tilde{\mathbf{v}} + \tilde{\mathbf{v}}\cdot\nabla\mathbf{v}_0 + (\tilde{\mathbf{v}}\cdot\nabla)\tilde{\mathbf{v}}\right) = -\frac{e}{m_\mathrm{i}}\nabla\phi. \tag{36}$$

We consider electrostatic perturbations, $\nabla\times\mathbf{E} = 0$, so that one can introduce a scalar potential for the perturbed ion flow

$$\tilde{\mathbf{v}} = -\nabla\tilde{\chi}. \tag{37}$$

This representation is exact in the linear electrostatic case, however nonlinear terms in equation (36) may not satisfy the relation (37). A more general form for the ion velocity would be $\tilde{\mathbf{v}} = -\nabla\tilde{\chi} + \nabla\times\psi$, where the vector function ψ describes the solenoidal part of the ion velocity. In many situations, the ion dynamics is determined by the ballistic acceleration in the static electric field $\mathbf{E}_0 = -\nabla\phi_0$ so that the corrections to (37) are small and can be considered in equation (36) perturbatively. The full range of the validity of the potential representation (37) needs further studies.

In the potential approximation, the full ion equations become

$$\left(\frac{\partial}{\partial t} + \mathbf{v}_0\cdot\nabla\right)\nabla^2\tilde{\chi} = \nabla^2\left(\frac{e}{m_\mathrm{i}}\phi + \frac{(\nabla\tilde{\chi})^2}{2}\right), \tag{38}$$

and

$$\left(\frac{\partial}{\partial t} + \mathbf{v}_0\cdot\nabla\right)\frac{\tilde{n}}{n_0} - \nabla\tilde{\chi}\cdot\frac{\nabla n_0}{n_0} - \nabla^2\tilde{\chi} - \frac{\tilde{n}}{n_0}\nabla^2\tilde{\chi} = 0. \tag{39}$$

3.2. Nonlinear model in the dimensionless form

For nonlinear simulations, equations (25), (38) and (39) are transformed into the dimensionless form

$$\partial_t n = -v_0\partial_x n + \rho_*\partial_x\chi + \theta + n\theta + \nabla n\cdot\nabla\chi - D_n\nabla^4 n, \tag{40}$$

$$\partial_t\theta = -v_0\partial_x\theta + \eta - n + \nabla^2(\nabla\chi)^2/2 - D_\theta\nabla^4\theta, \tag{41}$$

$$\partial_t\eta = -u_0\partial_y\eta + \rho_*\partial_y\phi - \nu_*(\eta - n) - \{\phi, n\} - \mu\{\phi, \nabla_\perp^2\phi\} + \mu\nabla\cdot\{\phi, \nabla_\perp n\} - D_\eta\nabla^4\eta. \tag{42}$$

Here $\nabla^2\chi = \theta$, and $n + \mu\nabla_\perp^2\phi - \mu\nabla^2 n = \eta$. Dimensionless variables are defined as follows $t' = \omega_{\mathrm{LH}}t, x' = x/\rho_{\mathrm{LH}}, \tilde{n}/n_0 = n', \theta = \omega_{\mathrm{LH}}\theta', e\phi/T_\mathrm{e} = \phi', \chi' = \chi/\left(\rho_{\mathrm{LH}}^2\omega_{\mathrm{LH}}\right)$. The dimensionless ion and electron velocities are defined as $u_0' = v_{E0}/(\omega_{\mathrm{LH}}\rho_{\mathrm{LH}})$ and $v_0' = v_{0\mathrm{i}}/(\rho_{\mathrm{LH}}\omega_{\mathrm{LH}})$. In what follows, the primes are omitted from the equations. The normalized Larmor radius and collisionality are introduced as $\rho_* = \rho_{\mathrm{LH}}/L_n$ and $\nu_* = \nu/\omega_{\mathrm{LH}}$, $c_{\mathrm{LH}} = T_\mathrm{e}/\sqrt{m_\mathrm{e}m_\mathrm{i}}$, $\rho_{\mathrm{LH}} = c_{\mathrm{LH}}/\omega_{\mathrm{LH}}$, $\mu = \sqrt{m_\mathrm{e}/m_\mathrm{i}}$, D_n, D_θ, D_η are hyper-viscosity terms. All variables are considered on the rectangular two-dimensional periodic domain (x, y); $0\leqslant x < L_x$ and $0\leqslant y < L_y$, where x and y are the axial and azimuthal coordinates for the Hall thruster geometry. We consider uniform magnetic field, uniform electric field and fixed density gradient.

3.3. Nonlinear simulations

The fluid simulations presented in this paper are performed in the BOUT++ framework that was adapted for simulations of partially magnetized plasmas of for $\mathbf{E}\times\mathbf{B}$ discharges [56]. BOUT++ was developed [91] for fluid and plasma simulations in curvilinear magnetic field geometry using finite-difference discretization and a variety of numerical methods and time-integration solvers. It was designed and tested with reduced plasma fluid models applications and has been widely used for studies of edge tokamak phenomena, 3D plasma turbulence and structures [92–94].

The typical parameters [65] for nonlinear simulations reported in this paper are as follows: $T_\mathrm{e} = 20$ eV, $n_0 = 10^{18}$ m^{-3}, $B_0 = 10^{-2}$ T, $E_0 = 10^4$ V m^{-1}, $m_\mathrm{i} = 131$ amu (Xe+), $\omega_{\mathrm{LH}} = 3.6\cdot 10^6$ rad s^{-1}, $c_{\mathrm{LH}} = 8.485\cdot 10^4$ m s^{-1}, $\rho_{\mathrm{LH}} = 2.35$ cm, $v_0 = 0.35\ c_{\mathrm{LH}}$, $u_0 = 11.7\ c_{\mathrm{LH}}$, $\nu_\mathrm{e} = 0.1826\ \omega_{\mathrm{LH}}$, $D = D_n = D_\theta = D_\eta = 10^{-6}$. Number of points in the axial direction (x) is 1320, and number of points in azimuthal directions is 128.

The BOUT++ initial simulations were benchmarked in the linear regime by using the initial condition in the form $\sim \sin(2\pi x/L_x)\sin(2\pi y/L_y)$. The comparison with the linear eigen-value solutions is shown in figure 5. In nonlinear simulations the linear (exponential) instability phase lasts few $\tau_{\mathrm{LH}} = \omega_{\mathrm{LH}}^{-1}$ periods. The simulations were run for $30\tau_{\mathrm{LH}}$ corresponding to 300 time steps. As the amplitude of fluctuations exponentially increases, nonlinear effects come into play, and instabilities reach saturation at $t = 5$–$10\ \tau_{\mathrm{LH}}$, figure 6. The nonlinear saturation has been monitored via the 'energy-like' functionals $E_f \equiv E[f(x,y)] = \int f(x,y)^2\mathrm{d}x\mathrm{d}y$, where $f = (n, \phi)$ and the integration is performed over the whole domain. In the saturated state, the energy input into the system due to the equilibrium density gradient and $\mathbf{E}\times\mathbf{B}$ flow (which are the main sources of the instability) are balanced by the sink due to the dissipation and hyperviscosity. We have confirmed in simulations with different time and spatial resolution that the average amplitudes of fluctuating quantities: density, velocity potential χ and electrostatic potential ϕ, as well as the average value of the nonlinear electron current are not affected by initial conditions nor by the value of the hyper-viscosity. We do observe a slow secondary growth of quadratic E_n and E_ϕ integrals, more pronounced for E_n rather for E_ϕ in figure 6. The nature of this slow growth is being investigated now in longer simulations with increased resolution. One can expect that the kinetic energy of ions $E_\mathrm{i} = m_\mathrm{i}\int n(\nabla\chi)^2\mathrm{d}x\mathrm{d}y$, and electrons $E_\mathrm{e} = m_\mathrm{e}c^2/B_0^2\int n(\nabla\phi)^2\mathrm{d}x\mathrm{d}y$ should form the basic quadratic conserved quantities. It is interesting that for cold electrons, the nonlinear terms in potential vorticity equation (42) conserve the enstrophy–like integral $I = \int\eta^2\mathrm{d}x\mathrm{d}y$, where $\eta = n + \nabla^2\phi$ is the potential vorticity for cold electrons. The

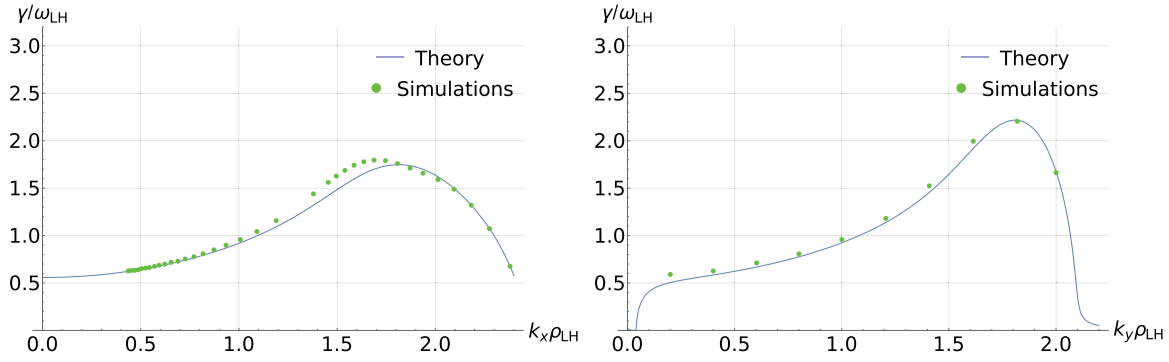

Figure 5. The linear benchmark of the BOUT++ initial value simulations against the linear analytical eigen-value solutions from equations (40)–(42), $k_y\rho_{\rm LH} = 1$, and $k_x\rho_{\rm LH} = 1$, for each plot respectively.

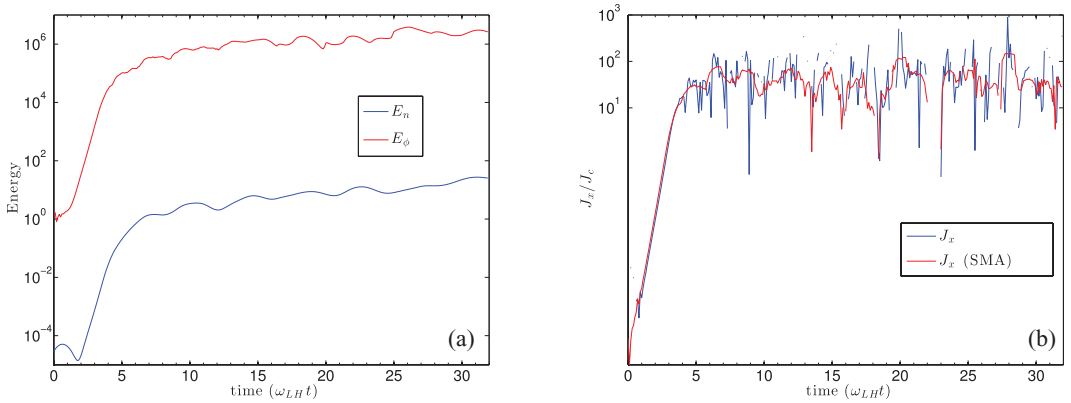

Figure 6. (a) Evolution of energy-like integrals during linear stage of the instability and nonlinear saturation. (b) Normalized anomalous current in nonlinear simulations. The standard moving average (SMA) is also shown, averaging is done over 10 $\omega_{\rm LH}^{-1}$.

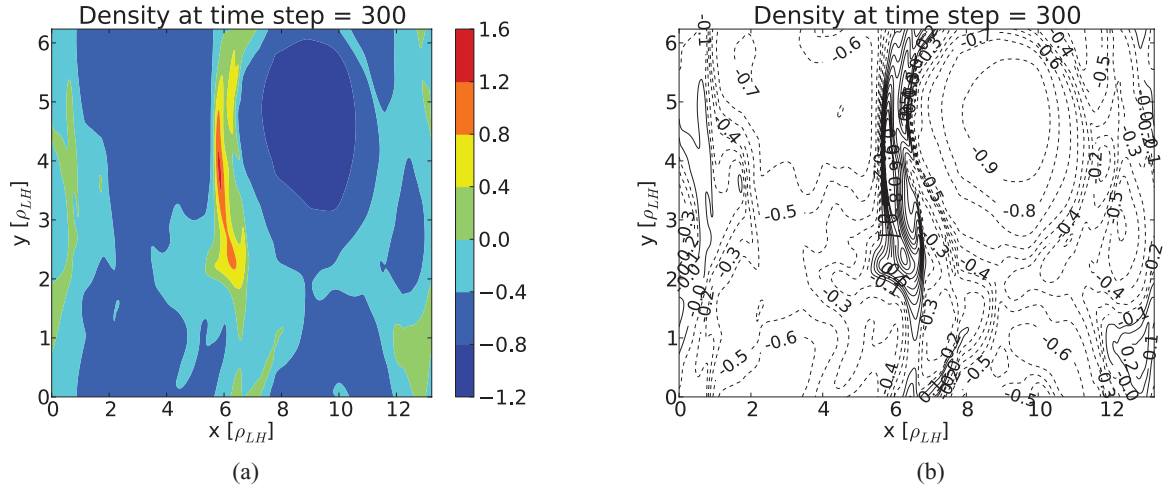

Figure 7. Perturbed plasma density at $t = 30\omega_{\rm LH} = 300$ time steps. (a) Colour coded levels of constant $\tilde{n}/n_0$. (b) The solid lines show levels of positive $\tilde{n}/n_0$, dotted lines- negative.

structure of the quadratic conserved quantities in the nonlinear system (40)–(42) and their relations with physical energy integrals will be investigated further.

Nonlinear cascade creates modes with high wave numbers. The small-scale modes below the smallest spatial length scale in the simulations have to be removed from the system to avoid numerical instability. The standard approach in nonlinear turbulence simulations is to introduce artificial hyper-viscosity terms to damp such modes. We have varied the magnitude of the hyper-viscosity D and have found that for the broad range of the values of the hyper-viscosity $D \leqslant 10^{-4}$ the saturation level and linear growth region are not affected.

One of the important results of our simulations is the demonstration of the anomalous electron current due to turbulent fluctuation. The anomalous current is calculated as an average $J_x = \langle \tilde{n}\widetilde{V}_{\rm Ex}\rangle = L_x^{-1}L_y^{-1}cB_0^{-1}\int n\partial_y\phi {\rm d}x{\rm d}y$. The value of the turbulent current is shown in figure 6(b) in units of the classical collisional current, $J_{\rm c} = en_0\nu_{\rm e}E_0/(B_0\omega_{\rm ce})$. For the

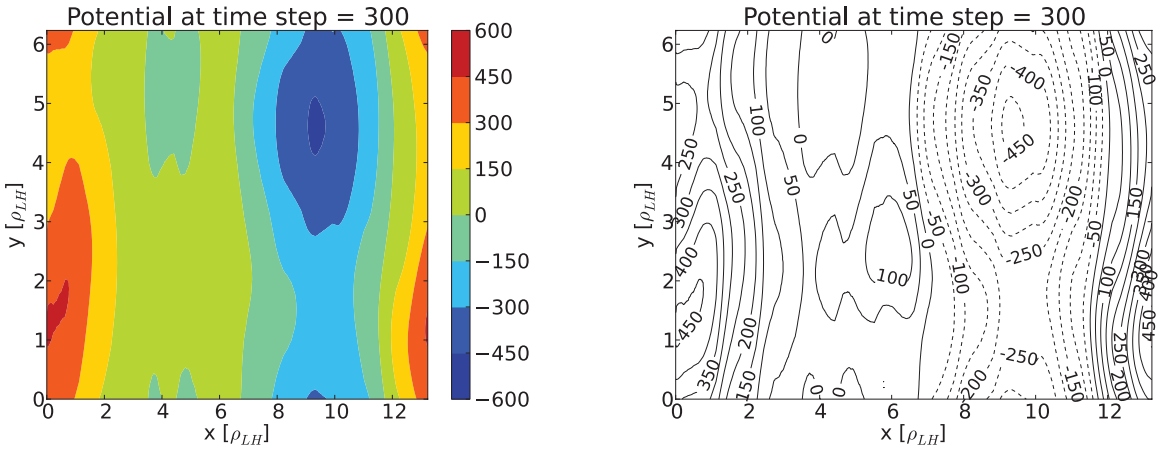

Figure 8. Normalized perturbed plasma potential at $t = 30\omega_{\mathrm{LH}}$ show levels of positive $e\phi/T_e$, dotted lines- negative.

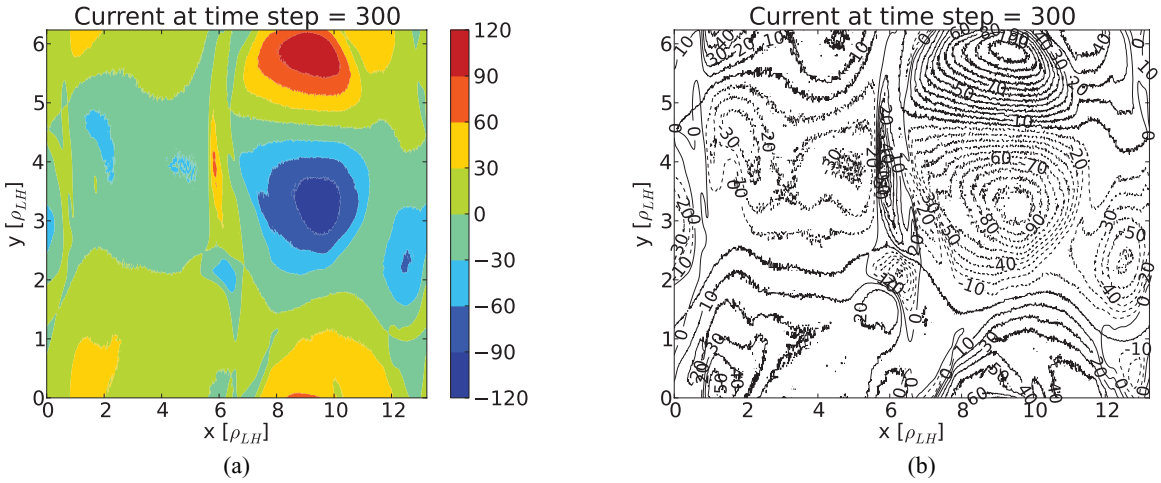

Figure 9. Normalized turbulent current at $t = 30\omega_{\mathrm{LH}}$. (a) Colour coded levels of constant J/J_c. (b) The solid lines show levels of positive J/J_c, dotted lines- negative.

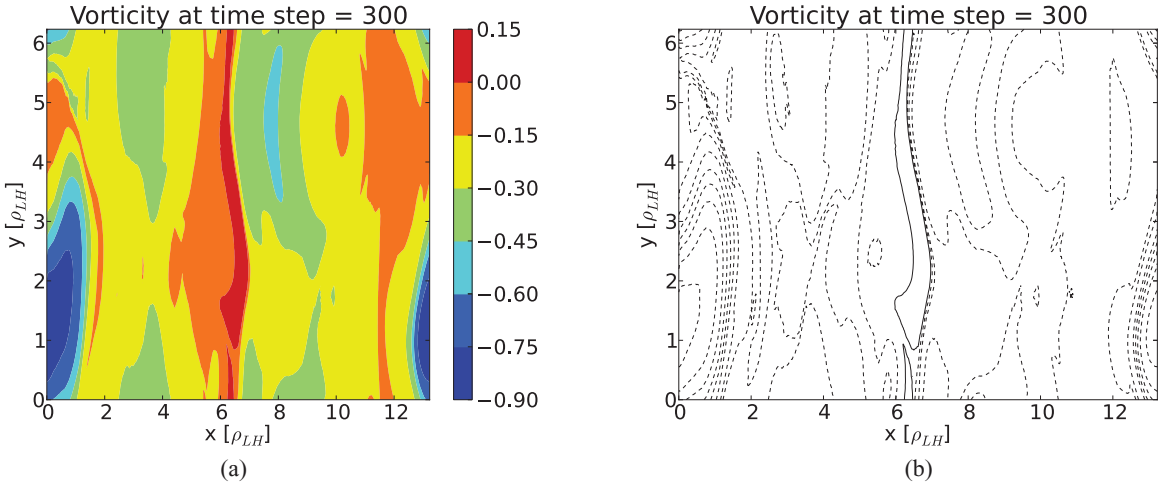

Figure 10. Generalized vorticity at $t = 30\omega_{\mathrm{LH}}$. (a) Colour coded levels of constant η. (b) The solid lines show levels of positive vorticity, dotted lines- negative, the absolute values are as in colour bar in (a).

parameters of our nonlinear simulations, the anomalous current $J_x \simeq 10^2\, J_c$, corresponds to the effective Hall parameter $\Omega_H \simeq 27$, $\Omega_H = \omega_{ce}/\nu_{\mathrm{eff}}$. Thus the values of the anomalous current J_x in the range of $50 \div 100\, J_c$, obtained in nonlinear simulations, figure 6(b), correspond to $\Omega_H = 54 \div 27$. These values roughly correspond to the values obtained in experiments with Penning discharges [23] and in PIC simulations [58].

As is shown in figure 6(b), the turbulent current is highly intermittent in time and space. Such intermittency may be related to the presence of coherent structures in turbulence. Figures 7 and 8 clearly show the relatively large structures of the order of few ρ_{LH} moving in the azimuthal direction. The anomalous current is a result of the phase shift between density and potential, $J_x \sim \langle \tilde{n}\partial\tilde{\phi}/\partial y\rangle$. In quasilinear regime this phase shift can be estimated from the linear growth rate: $\gamma\tilde{n} \simeq \tilde{\mathbf{v}}_E \cdot \nabla n_0$. In the nonlinear regime the linear growth rate should be replaced with the nonlinear broadening frequency, $\Delta\omega_{nl}$. In the nonlinear saturation state, the nonlinear broadening frequency is of the order of the lower-hybrid frequency, $\Delta\omega_{nl} \simeq \omega_{\mathrm{LH}}$.

The resulting structure of the current in shown in figure 9. Note that, the current in this figure is along the x-direction. It is easily observed that the maximum of the turbulent current in figure 9 is well correlated with the density and potential structures. The vorticity in figure 10 also shows a similar structure though less pronounced. In the saturated state, as shown in figures 7 and 8, the maximum amplitude of the density fluctuations $\tilde{n}/n_0 \simeq 0.2$ and the fluctuating electric field is slightly larger than the equilibrium field, $\widetilde{E} \geqslant E_0$.

The anomalous current and coherent structures observed in our simulations are reminiscent to azimuthally rotating structures observed in Hall thrusters and magnetrons [95, 96]. It has been confirmed experimentally that the signficant part of the anomalous current is carried by the spoke [5]. The appearance of spokes in Hall plasma turbulence was noted long time ago [97] and they remain to be regular features of Hall thruster [20–22, 98] and magnetron operation [95, 96], however, the mechanism of spoke formation is still not clear. The spoke could be a result of turbulence nonlinear self-organisation rather than directly originate from some linear instability. It has been suggested that modulational instability of lower-hybrid modes may result in large scale low frequency coherent modes [99]. The tendency toward formation of coherent structures in our simulations may be associated with the above noted conservation of the enstrophy–like integral. This phenomena requires further studies.

4. Summary

In this paper, an advanced fluid model for Hall plasmas with magnetized electrons and unmagnetized fluid ions has been developed. A general overview of the instabilities in partially-magnetized plasmas relevant to electric propulsion and magnetron devices for material processing has been provided using this fluid model. The electron description is based on the low frequency ($\omega < \omega_{\mathrm{ce}}$) reduction of the electron dynamics taking into account electron inertia and gyroviscosity. The model extends the collisionless Simon-Hoh instability into the short wavelength and higher frequency regimes that include the lower-hybrid modes. It is shown that the lower-hybrid mode destabilized by the density gradient is a natural extention of the Simon-Hoh instability. The gyro viscosity effects, which are of the same order as the electron inertia, are important for plasmas with finite electron temperature. The lower-hybrid modes in plasmas $\mathbf{E} \times \mathbf{B}$ drift can be destabilized by the density gradient as well as electron-neutral collisions which are especially effective at shorter wave-lengths. The effects of the gyroviscosity describe the transition of the lower-hybrid waves into the ion sound waves for $k_\perp^2\rho_{\mathrm{e}}^2 \gg 1$.

The reduced nonlinear fluid model has been implemented in the high performance BOUT++ framework. Initial value simulations have been bench marked in the linear regime against the results obtained by the eigenvalue solvers. In nonlinear simulations, the saturation of turbulence and formation of the coherent structures have been demonstrated. It is shown that the instability reaches the saturation in nonlinear regime at a level which is independent of the initial state. Significant anomalous current due to turbulent fluctuations has been found in the nonlinear state. The anomalous (turbulent) current is strongly intermittent and the structures observed in the current density are well correlated with density and potential structures. The density and current structures are reminiscent of experimentally observed structures (spokes) in Hall thrusters and magnetrons and the values of the anomalous Hall parameter are consistent with experiments in Penning discharge and PIC simulations.

The nonlinear model and simulations presented in this paper provide the first principles calculations of the anomalous electron current from turbulent fluctuations. Further work will include expansion of the model to include ionization [61, 62] and 3D geometry effects as well as self-consistent multi-scale simulations allowing for slow evolution of background plasma parameters.

Acknowledgments

This work is supported in part by NSERC Canada, US Air Force Office of Scientific Research FA9550-15-1-0226 and Russian Foundation for Basic Research (Grant No. 16-02-00640). The authors acknowledge useful discussions with I Khalzov, V I Ilgisonis, E Sorokina, and M Cappelli.

References

[1] Morozov A and Savelyev V 2000 Fundamentals of stationary plasma thruster theory, in *Reviews of Plasma Physics* vol 21, ed B Kadomtsev and V Shafranov (New York: Kluver) p 203
[2] Cappelli M 2009 *Phys. Today* **62** 76–7
[3] Abolmasov S N 2012 *Plasma Sources Sci. Technol.* **21** 035006
[4] Boeuf J P, Claustre J, Chaudhury B and Fubiani G 2012 *Phys. Plasmas* **19** 113510
[5] Ellison C L, Raitses Y and Fisch N J 2012 *Phys. Plasmas* **19** 013503
[6] Amatucci W E, Ganguli G, Walker D N, Gatling G, Balkey M and McCulloch T 2003 *Phys. Plasmas* **10** 1963–70
[7] Koepke M E, Amatucci W E, Carroll J J and Sheridan T E 1994 *Phys. Rev. Lett.* **72** 3355–8
[8] DuBois A M, Thomas E, Amatucci W E and Ganguli G 2014 *Phys. Plasmas* **21** 062117
[9] Koo J W and Boyd I D 2006 *Phys. Plasmas* **13** 033501
[10] Keidar M and Beilis I 2006 *IEEE Trans. Plasma Sci.* **34** 804–14
[11] Lazurenko A, Coduti G, Mazouffre S and Bonhomme G 2008 *Phys. Plasmas* **15** 034502

[12] Spector R A 2007 *Int. Electric Propulsion Conf. (Florence, Italy)* IEPC-2001-70
[13] Meezan N B, Hargus W A and Cappelli M A 2001 *Phys. Rev.* E **63** 026410
[14] Fernandez E, Scharfe M K, Thomas C A, Gascon N and Cappelli M A 2008 *Phys. Plasmas* **15** 012102
[15] Boniface C, Garrigues L, Hagelaar G J M, Boeuf J P, Gawron D and Mazouffre S 2006 *Appl. Phys. Lett.* **89** 161503
[16] Tilinin G N 1977 *Sov. Phys. Tech. Phys.* **22** 974–8
[17] Choueiri E Y 1999 *Phys. Plasmas* **6** 2290–306
[18] Lazurenko A, Albarede L and Bouchoule A 2006 *Phys. Plasmas* **13** 083503
[19] Tsikata S, Lemoine N, Pisarev V and Gresillon D M 2009 *Phys. Plasmas* **16** 033506
[20] Sekerak M J, Longmier B W, Gallimore A D, Brown D L, Hofer R R and Polk J E 2015 *IEEE Trans. Plasma Sci.* **43** 72–85
[21] Sekerak M, Longmier B, Gallimore A D, Brown D L, Hofer R and Polk J E 2013 *Int. Electric Propulsion Conf. (Washington D.C., USA)* IEPC-2013-143
[22] Parker J B, Raitses Y and Fisch N J 2010 *Appl. Phys. Lett.* **97** 091501
[23] Raitses E, Kaganovich I and Smolyakov A I 2015 *Int. Electric Propulsion Conf. (Hyogo-Kobe, Japan)* IEPC-2015-307
[24] Mikhailovskii A B 1992 *Electromagnetic Instabilities in an Inhomogeneous Plasma* (London: Taylor and Francis)
[25] Fridman A M 1964 *Sov. Phys.—Dokl.* **9**
[26] Krall N A and Liewer P C 1971 *Phys. Rev.* A **4** 2094
[27] Stepanov K N 1965 *Sov. Phys. Tech. Phys.-USSR* **9** 1653
[28] Mikhailovskii A B and Tsypin V S 1966 *Sov. Phys. JETP Lett.* **3** 158–9
[29] Morozov A I, Esipchuk Y V, Kapulkin A, Nevrovskii V and Smirnov V A 1972 *Sov. Phys. Tech. Phys.* **17** 482–7
[30] Esipchuk Y V and Tilinin G N 1976 *Sov. Phys. Tech. Phys.* **21** 417–23
[31] Gorshkov O A, Tomilin D A and Shagaida A A 2012 *Plasma Phys. Rep.* **38** 271–7
[32] Tomilin D 2013 *Phys. Plasmas* **20** 042103
[33] Sakawa Y, Joshi C, Kaw P K, Chen F F and Jain V K 1993 *Phys. Fluids* B **5** 1681–94
[34] Simon A 1963 *Phys. Fluids* **6** 382–8
[35] Hoh F C 1963 *Phys. Fluids* **6** 1184–91
[36] Huba J D and Wu C S 1976 *Phys. Fluids* **19** 988–94
[37] Krall N A and McBride J B 1976 *Phys. Fluids* **19** 1970–1
[38] Davidson R C and Gladd N T 1975 *Phys. Fluids* **18** 1327–35
[39] Fruchtman A 1989 *Phys. Fluids* B **1** 422–9
[40] Lampe M, Manheime W M, McBride J B, Orens J H, Shanny R and Sudan R N 1971 *Phys. Rev. Lett.* **26** 1221
[41] McBride J B, Ott E, Boris J P and Orens J H 1972 *Phys. Fluids* **15** 2367–83
[42] Ducrocq A, Adam J C, Heron A and Laval G 2006 *Phys. Plasmas* **13** 102111
[43] Lominadze D G 1972 *Zh. Eksp. Teor. Fiz.* **63** 1300
[44] Cavalier J, Lemoine N, Bonhomme G, Tsikata S, Honore C and Gresillon D 2013 *Phys. Plasmas* **20** 082107
[45] Adam J C, Heron A and Laval G 2004 *Phys. Plasmas* **11** 295–305
[46] Lafleur T, Baalrud S D and Chabert P 2016 *Phys. Plasmas* **23** 053502
[47] Lafleur T, Baalrud S D and Chabert P 2016 *Phys. Plasmas* **23** 053503
[48] Boeuf J P A 2016 Physics and Modeling of Hall Effect Thrusters, von Karman Institute for Fluid Dynamics Lecture Series (Von Karman Institute, Belgium, 2016), submitted to *J. Appl. Phys.* STO-AVT-263
[49] Smolyakov A I, Frias W, Kaganovich I D and Raitses Y 2013 *Phys. Rev. Lett.* **111** 115002
[50] Kadomtsev B 1965 Plasma instability *7th Conf. on Phenomena in Ionized Gases* vol 2 (Belgrade: Consultants Bureau) p 610
[51] Chen F F 1979 *Phys. Fluids* **22** 2346–58
[52] Matyash K, Schneider R, Mazouffre S, Tsikata S, Raitses E and Diallo A 2013 *Int. Electric Propulsion Conf. (Washington DC, USA)* IEPC-2013-307
[53] Taccogna F, Longo S, Capitelli M and Schneider R 2009 *Appl. Phys. Lett.* **94** 251502
[54] Coche P and Garrigues L 2014 *Phys. Plasmas* **21** 023503
[55] Boeuf J P and Chaudhury B 2013 *Phys. Rev. Lett.* **111** 155005
[56] Frias W, Smolyakov A I, Kaganovich I D, Raitses Y and Umansky M 2012 Simulation of gradient drift instabilities in Hall thruster plasmas with the BOUT++ code *54th Annual Meeting of the APS Division of Plasma Physics (Providence, Rhode Island) vol* 57 BAPS.2012.DPP. YP8.68
[57] Pombo F W, Smolyakov A I, Romadanov I, Raitses E, Kaganovich I and Umansky M 2015 *Int. Electric Propulsion Conf. (Hyogo-Kobe)* IEPC-2015-370
[58] Carlsson J, Kaganovich I, Khrabrov A, Raitses E and Sydorenko D 2015 *Int. Electric Propulsion Conf. (Hyogo-Kobe, Japan)* IEPC-2015-373
[59] Gladd N T 1976 *Plasma Phys. Control. Fusion* **18** 27–40
[60] Barral S and Ahedo E 2008 On the origin of low frequency oscillations in hall thrusters *Plasma 2007* (*AIP Conf. Proc.* vol 993) ed H J Hartfuss (Melville, NY: American Institute of Physics) pp 439–42
[61] Escobar D and Ahedo E 2014 *Phys. Plasmas* **21** 043505
[62] Escobar D and Ahedo E 2015 *Phys. Plasmas* **22** 102114
[63] Wei L Q, Han L, Yu D R and Guo N 2015 *Chin. Phys.* B **24** 055201
[64] Litvak A A, Raitses Y and Fisch N J 2004 *Phys. Plasmas* **11** 1701–5
[65] Smirnov A, Raitses Y and Fisch N J 2004 *J. Appl. Phys.* **95** 2283
[66] Jorns B A and Hofer R R 2014 *Phys. Plasmas* **21** 053512
[67] Ito T, Young C V and Cappelli M A 2015 *Appl. Phys. Lett.* **106** 254104
[68] Jaeger S, Pierre T and Rebont C 2009 *Phys. Plasmas* **16** 022304
[69] Romadanov I, Smolyakov A I, Raitses E, Kaganovich I and Ryzhkov S 2016 Structure of unstable nonlocal gradient-drift modes in Hall ExB discharges, submitted to *Phys. Plasmas*
[70] Romadanov I, Smolyakov A I, Frias W, Chapurin O and Koshkarov O 2016 arXiv:1680435
[71] Tao Y Q, Conn R W, Schmitz L and Tynan G 1993 *Phys. Fluids* B **5** 344–9
[72] Tao Y Q, Conn R W, Schmitz L and Tynan G 1994 *Phys. Plasmas* **1** 3193–8
[73] Sakawa Y, Joshi C, Kaw P K, Jain V K, Johnston T W, Chen F F and Dawson J M 1992 *Phys. Rev. Lett.* **69** 85–8
[74] Chen F F and Hsieh M 1993 *Proc. Int'l Workshop on Magnetic Turbulence and Transport (Cargese, France)* pp 56–69 $\mathbf{E} \times \mathbf{B}$ instability in regions of strong electric shear UCLA, PPG-1465
[75] Chen F F 1992 *Proc. Int'l Workshop on Magnetic Turbulence and Transport (Cargese, France)* pp 56–69 A collisionless E × B instability with large ion orbits, UCLA PPG-1434
[76] Frias W, Smolyakov A, Kaganovich I and Raitses Y 2013 *Phys. Plasmas* **20** 052108
[77] Frias W, Smolyakov A, Kaganovich I D and Raitses Y 2014 *Phys. Plasmas* **21** 062113
[78] Pogutse I O, Smolyakov A I and Hirose A 1998 *J. Plasma Phys.* **60** 133–49
[79] Mikhailovskii A B and Tsypin V S 1984 *Beitrage Plasmaphys.* **24** 335–54
[80] Smolyakov A I 1998 *Can. J. Phys.* **76** 321–31
[81] Hsu C T, Hazeltine R D and Morrison P J 1986 *Phys. Fluids* **29** 1480–7
[82] Litvak A A and Fisch N J 2004 *Phys. Plasmas* **11** 1379–83

[83] Kapulkin A and Guelman M 2005 *29th Int. Electric Propulsion Conf. (Princeton, New Jersey) p* 88
[84] Litvak A A and Fisch N J 2001 *Phys. Plasmas* **8** 648–51
[85] Huba J D and Ossakow S L 1979 *Phys. Fluids* **22** 1349–54
[86] Lampe M, McBride J B, Orens J H and Sudan R N 1971 *Phys. Lett.* A **35** 131
[87] Lashmore C and Martin T J 1973 *Nucl. Fusion* **13** 193–203
[88] Koshkarov O, Smolyakov A I, Kaganovich I D and Ilgisonis V I 2015 *Phys. Plasmas* **22** 052113
[89] Kapulkin A and Guelman M M 2008 *IEEE Trans. Plasma Sci.* **36** 2082–7
[90] Frias W, Smolyakov A I, Kaganovich I D and Raitses Y 2012 *Phys. Plasmas* **19** 072112
[91] Dudson B D, Umansky M V, Xu X Q, Snyder P B and Wilson H R 2009 *Comput. Phys. Commun.* **180** 1467–80
[92] Angus J R, Umansky M and Krasheninnikov S I 2012 *Contrib. Plasma Phys.* **52** 348–52
[93] Popovich P, Umansky M V, Carter T A and Friedman B 2010 *Phys. Plasmas* **17** 122312
[94] Umansky M V, Popovich P, Carter T A, Friedman B and Nevins W M 2011 *Phys. Plasmas* **18** 055709
[95] Anders A, Ni P and Rauch A 2012 *J. Appl. Phys.* **111** 053304
[96] Brenning N, Lundin D, Minea T, Costin C and Vitelaru C 2013 *J. Phys. D: Appl. Phys.* **46** 084005
[97] Janes G S and Lowder R S 1966 *Phys. Fluids* **9** 1115
[98] Chesta E, Meezan N B and Cappelli M A 2001 *J. Appl. Phys.* **89** 3099–107
[99] Lakhin V, Ilgisonis V I, Smolyakov A I and Sorokina E A 2016 *Phys. Plasmas* **23** 102304